

Active particles in heterogeneous media display new physics

existence of an optimal noise and absence of bands and long-range order

Oleksandr Chepizhko^{1,2,a} and Fernando Peruani^{1,b}

¹ Laboratoire J.A. Dieudonné, Université de Nice Sophia Antipolis, UMR 7351 CNRS, Parc Valrose, F-06108 Nice Cedex 02, France

² Department for Theoretical Physics, Odessa National University, Dvoryanskaya 2, 65026 Odessa, Ukraine

Abstract. We present a detailed study of the large-scale collective properties of self-propelled particles (SPPs) moving in two-dimensional heterogeneous spaces. The impact of spatial heterogeneities on the ordered, collectively moving phase is investigated. We show that for strong enough spatial heterogeneity, the well-documented high-density, high-ordered propagating bands that emerge in homogeneous space disappears. Moreover, the ordered phase does not exhibit long-range order, as occurs in homogeneous systems, but rather quasi-long range order: i.e. the SPP system becomes disordered in the thermodynamical limit. For finite size systems, we find that there is an optimal noise value that maximizes order. Interestingly, the system becomes disordered in two limits, for high noise values as well as for vanishing noise. This remarkable finding strongly suggests the existence of two critical points, instead of only one, associated to the collective motion transition. Density fluctuations are consistent with these observations, being higher and anomalously strong at the optimal noise, and decreasing and crossing over to normal for high and low noise values. Collective properties are investigated in static as well as dynamic heterogeneous environments, and by changing the symmetry of the velocity alignment mechanism of the SPPs.

1 Introduction

We understand by an *active particle*, a particle that is able to convert energy into work to self-propel in a dissipative medium. There are several strategies to achieve self-propulsion. (i) Particles may possess an energy depot and being equipped with a motor ¹, a scenario representative of many biological systems such as moving bac-

^a e-mail: oleksandr.chepizhko@gmail.com

^b e-mail: peruani@unice.fr

¹ Motility assays represent a particular case, where motors are not attached to the moving particles, while the energy depot could be considered as extended over the space [1]

teria [2,3], insects [4,5], and animals [6,7]. (ii) Particles may be able to rectify an external driving in order to achieve self-propulsion in a given direction, a situation commonly observed in non-living, artificial active particles such as vibration-induced self-propelled rods and discs [8,9,10], light-induced thermophoretic active particles [11,12,13,14], chemically driven particles [15,16,17,18,19,20], and rollers driven by the Quicke rotation effect [21]. Independently of the strategy exploited by the particles to self-propel, these systems are intrinsically out of (thermodynamic) equilibrium² and even in absence of particle-particle interactions exhibit a non-trivial behavior. For instance, fluctuations in the self-propelling mechanism can lead to complex transients in the mean-square displacement of the particles [22] as well as anomalous velocity distributions [23].

Interestingly, most, if not all, active particle systems found in nature take place, at all scales, in the heterogeneous media: from the active transport inside the cell [24], that is filled by organelles and vesicles, and bacterial motion in natural habitats [25], such as the gastrointestinal tract and the soil, among other complex environments, to the migration of herd of mammals across forests and steppes [7]. Despite this evident fact, active matter research has focused almost exclusively, at the experimental and theoretical level, on homogeneous active systems [26,27,28,23,29]. Non-equilibrium, large-scale properties of active systems such as long-range order in two-dimensions as Vicsek et al. [30] reported in their pioneering paper, the emergence of high-order, high-density traveling bands [31,32], and the presence of giant number fluctuations in ordered phases [27,33,34] are all non-equilibrium features either predicted or discovered in perfectly homogeneous systems. Here, we show that most of these non-equilibrium features are strongly affected by the presence of spatial heterogeneities. Moreover, we show that these properties vanish in strongly heterogeneous media. More specifically, we extend previous results [35] on the large-scale collective properties of interacting self-propelled particles (SPPs) moving at constant speed in an heterogeneous space. We model the spatial heterogeneity as a random distribution of undesirable areas or “obstacles” that the SPPs avoid. The degree of heterogeneity is controlled by the average density ρ_o of obstacles. We provide numerical evidence that indicates that at low densities of heterogeneities ρ_o , the SPPs exhibit, below a critical noise intensity η_{c1} , long-range order (LRO). For noise intensities η close to η_{c1} , the SPPs self-organize, as in homogeneous spaces, into high-density traveling structures called “bands”. We find that as ρ_o is increased, bands become less pronounced to the point that for large enough values of ρ_o they are no longer observed. Our results indicate that in strongly heterogeneous media, i.e. large values of ρ_o , the large-scale properties of the system are remarkably different from what we know of the Vicsek model [30] in two-dimensional homogeneous media. For instance, orientational order for $\eta < \eta_{c1}$ is no longer LRO, but rather quasi-long range (QLRO), with the system exhibiting the maximum degree of order at an intermediate noise value η_M , such that $0 < \eta_M < \eta_{c1}$. Moreover, we provide solid evidence that the system becomes disordered as $\eta \rightarrow 0$. The numerical data suggests the existence of a second critical point η_{c2} , with $0 < \eta_{c2} < \eta_{c1}$ below which the system is genuinely disordered. The disordered phase at low η values is characterized by the presence of large, dense moving clusters. We show that the particle number statistics is consistent with these observations: giant number fluctuations (GNF) peak at η_M and decrease as η approaches η_{c2} , with GNF becoming weaker as ρ_o is increased to the point that fluctuations become normal. Finally, we investigate and compare static and dynamical heterogeneous media, as well as SPPs with ferromagnetic and nematic velocity alignment. We show that in all cases there exists an optimal noise intensity that maximizes the ordering

² This is due to the energy consumption involved by the self-propelling mechanism and the energy dissipated to the medium

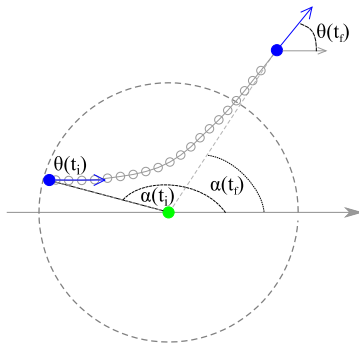


Fig. 1. Interaction of a self-propelled particle (blue) with an obstacle (green). Angles are given with respect to horizontal axis that is directed from left to right. The moving direction given by the angle $\theta(t)$ evolves in time from an initial direction at t_i to a final direction at t_f final. The temporal evolution of the particle, with respect to the obstacles, is given by the angle $\alpha(t)$. The initial value of α at t_i is marked with blue dashed line and its final value at t_f is marked with a dark green dashed line. Notice, that after a collision, $\theta(t_f) \approx \alpha(t_f)$, the difference $\Delta = \theta(t_f) - \alpha(t_f)$ is such that $\Delta \ll 1$ for either large values of γ_o or large values of R_o . In the figure, $\gamma_o = 1$ and $R_b = 1$.

in the systems. The reported results might be a great importance for the design and control of active particle system.

The paper is organized as follows. In Section 2 we introduce a general and minimal model for SPPs in heterogeneous media. The collective motion phase, the associated kinetic phase transition and ordering properties of the model are studied in Sec. 3. Anomalous density fluctuations are addressed in Sec. 4. In section 5, we investigate the collective properties of SPPs in a dynamical heterogeneous environment, and discuss the effect of the velocity alignment symmetry. We summarize our results in Sec. 6.

2 Formulation of the model

We consider a system of N self-propelled particles, moving with a constant speed v_0 on a two-dimensional heterogeneous space of linear size L with periodic boundary conditions. We express the equations of motion of the i -th particle as:

$$\dot{\mathbf{x}}_i = v_o \mathbf{V}(\theta_i) \quad (1)$$

$$\dot{\theta}_i = g(\mathbf{x}_i) \left[\frac{\gamma_b}{n_b(\mathbf{x}_i)} \sum_{|\mathbf{x}_i - \mathbf{x}_j| < R_b} \sin[q(\theta_j - \theta_i)] \right] + h(\mathbf{x}_i, \theta_i) + \eta \xi_i(t), \quad (2)$$

where the dot denotes temporal derivative, \mathbf{x}_i corresponds to the position of the i th particle, and θ_i is an angle associated to its moving direction. Equation (1) indicates simply that the particle moves at speed v_0 in direction $\mathbf{V}(\theta_i) = (\cos \theta_i, \sin \theta_i)$. Equation (2) conveys the dynamics of the moving direction of the particle, which is parametrized by the angle θ_i . The first term on the right-hand side corresponds to a velocity-velocity alignment mechanism acting between neighboring particles as in the Vicsek model [30], the second term models the interaction of the i -th particle with

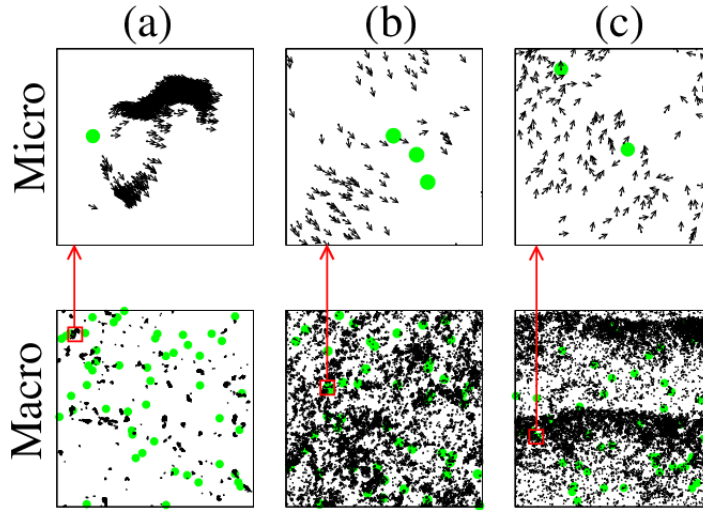


Fig. 2. Simulation snapshots of different phases for $\rho_o = 2.55 \times 10^{-3}$ for a system size $N_b = 19600$ ($L = 140$). The SPP are represented as black arrows, while the obstacles as green dots. The bottom panels correspond to macroscopic phases, while the top panels to zoom up regions, where the interaction between the SPP and the obstacles can be appreciated. From left to right: (a) clustered phase, $\eta = 0.01$ and $r = 0.58$, (b) homogeneous ordered phase, $\eta = 0.3$ and $r = 0.97$, and (c) ordered band phase, $\eta = 0.6$ and $r = 0.73$.

the spatial heterogeneities, and the third term is an additive noise, where $\langle \xi_i(t) \rangle = 0$, $\langle \xi_i(t) \xi_j(t') \rangle = \delta_{ij} \delta(t - t')$, and η denotes the noise strength. The velocity-velocity alignment is characterized by three parameters: its symmetry, given by q and that we fix for most of this analysis to be ferromagnetic with $q = 1$, the interaction radius R_b , and the alignment strength γ_b , where the symbol $n_b(\mathbf{x}_i)$ represents the number of SPPs at a distance less than or equal to R_b from \mathbf{x}_i , i.e. the number of neighbors of the i -th particle. The function $g(\mathbf{x}_i)$ controls the relative weight between alignment (to the other particles) and heterogeneity/obstacle avoidance. We tested two possibilities, both leading to the same macroscopic behavior: $g(\mathbf{x}_i) = 1$ and $g(\mathbf{x}_i) = 1 - \Theta(n_o(\mathbf{x}_i))$, where $\Theta(x)$ is Heaviside step function. The latter implies that in the proximity of an obstacle, the SP particle focuses on avoiding it, without aligning to the neighbors. Results shown here correspond to this definition. Finally, the interaction with the spatial heterogeneities, which we refer to as “obstacles” or undesirable areas, is given by the function $h(\mathbf{x}_i, \theta_i)$, defined as:

$$h(\mathbf{x}_i, \theta_i) = \frac{\gamma_o}{n_o(\mathbf{x}_i)} \sum_{|\mathbf{x}_i - \mathbf{y}_k| < R_o} \sin(\alpha_{k,i} - \theta_i) \quad (3)$$

if $n_o(\mathbf{x}_i) > 0$, and $h(\mathbf{x}_i) = 0$ otherwise, where $n_o(\mathbf{x}_i)$ represents the number obstacles at a distance less than or equal to R_o . The angle $\alpha_{k,i}$ is simply the angle of the polar representation of the vector $\mathbf{x}_i - \mathbf{y}_k = \Gamma_{k,i} (\cos \alpha_{k,i}, \sin \alpha_{k,i})$, where \mathbf{y}_k is the position of the k th-obstacle and $\Gamma_{k,i}$ is the norm of the vector. The position \mathbf{y}_k of obstacles, with $k \in [1, N_o]$, is random and homogeneously distributed in space. The interaction between a SPP and an obstacle is depicted in figure 1: as the particle approaches the obstacle, its trajectory is deflected. While here we focus mainly on “obstacles” whose position is fixed in time, we will also address briefly, at the end of the paper, the case of moving obstacle, i.e. free to diffusive around the space.

It is worth analyzing few simple limits of the model given by equations (1) and (2). For $\gamma_b = \gamma_o = 0$, the equations define a system of non-interacting persistent random

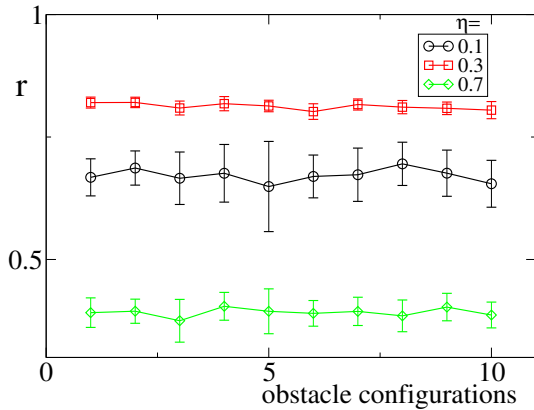


Fig. 3. Average values of order parameter r for 10 different initial configuration of obstacles for three values of the noise strength η and $\rho_o = 0.0325$. System size $N_b = 10000$. Notice that the average value of the order parameter does not depend on the particular configuration of the randomly placed (static) obstacles. The error bars correspond to the standard deviation of the time series of r obtained for each obstacle configuration and set of parameters.

walkers characterized by diffusion coefficient $D_x = v_o^2/\eta^2$. With $\gamma_o = 0$ and $\gamma_b > 0$ (or equivalently $\gamma_o > 0$ and $N_o = 0$), the model reduces to a continuous-time version [36] of the Vicsek model [30]. For $\gamma_o > 0$, $\gamma_b = 0$, and $N_o > 0$, the equations describe a system of non-interacting active particles moving at constant speed on an heterogeneous space, where several interesting non-equilibrium features can be observed [37]. At low obstacle density, particles move diffusively with a diffusion coefficient that is, interestingly, a non-monotonic function of the obstacle density that reaches a minimum at a given, non-trivial, non-zero obstacle density. On the other hand, at high obstacle density and for large enough interaction strength γ_b , spontaneous trapping of particles can occur. In this scenario, particles move sub-diffusively across the space, spending arbitrary long time in the spontaneously formed traps [37]. Here, we focus on the general scenario where $\gamma_o > 0$, $\gamma_b > 0$, and $N_o > 0$. We reduce the parameter space by fixing the following parameters: $R_b = R_o = 1$, $\gamma_b = \gamma_o = 1$, $\rho_b = N_b/L^2 = 1$, $v_o = 1$ and a discretization time step to $\Delta t = 0.1$. Notice that our main control parameters are the noise intensity η and the number of obstacles N_o or equivalently, the obstacles density $\rho_o = N_o/L^2$.

3 The order-disorder transition

The system exhibits three distinct macroscopic phases, for any given obstacle density $\rho_o > 0$, as we move from high to low noise amplitude η . At high noise values, particles are homogeneously distributed in space as a disordered gas of non-interacting particles. Below a critical noise value η_{c1} , the system undergoes a kinetic phase transition from the disordered gas to a (locally) ordered phase. For finite size systems, there is a symmetry breaking and the ordered phase implies the existence of a net flux of particles in a given direction, or equivalently the existence of a preferred direction of motion. For values close to onset of collective motion, i.e. close to η_{c1} , and for rather low values of ρ_o particles self-organize into high-density, high-order traveling structures called “bands”, as illustrated in Fig. 2(c). As η is decreased further, getting deeper in the ordered phase, bands disappear and we observe an ordered phase where particles are roughly homogeneously distributed in space, though anomalously large

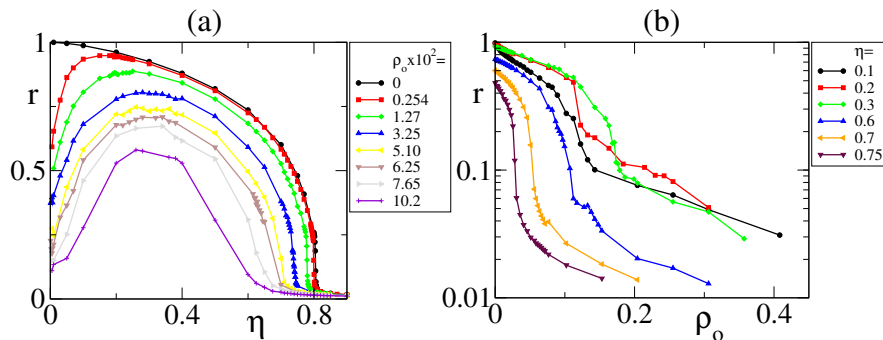


Fig. 4. (a) Order parameter r vs. noise strength η for various values of the obstacle density ρ_o . (b) Order parameter r vs. obstacle density ρ_o for various values of noise strength η . System size: $N_b = 19600$ ($L = 140$). Notice in (a) that curves for $\rho_o >$ exhibit a (local) maximum. This implies the existence of optimal noise value that maximizes collective motion.

density fluctuations are present, Fig. 2(b). If η is decreased even further, coming close to the noiseless limit, counterintuitively the degree of order drops dramatically and particles are organized into densely packed moving clusters, see Fig. 2(a), that are only weakly correlated due to the constant deflections they experience when running into obstacles.

In order to quantify the degree of order in the system, we use the following order parameter:

$$r = \langle r(t) \rangle_t = \left\langle \left| \frac{1}{N_b} \sum_{i=1}^{N_b} e^{i\theta_i(t)} \right| \right\rangle_t, \quad (4)$$

where $\langle \dots \rangle_t$ denotes the average over time³. The definition of r is simply, in complex notation, the norm of the average velocity of the particles. Values of r larger than zero indicate that there is a net flux of particles in a given direction, while $r = 0$ corresponds to a disordered system. It is important to stress that average value of r does not depend on the particular configuration of (static) obstacles, as long as the obstacles have been placed randomly in the space. For instance, if we compare simulations performed with different obstacle configurations, we obtain the same average value of r , as shown in Fig. 3, where the error bars represent the measured standard deviation in the corresponding time series of the order parameter r . In summary, the value of r , Eq. 4, depends only on the noise amplitude η and obstacle density ρ_o .

Fig. 4 shows the dependency of the order parameter r with respect to the noise intensity η for various obstacle densities ρ_o , panel (a), and with respect to the obstacle density for various noise intensities, panel (b). The curve that corresponds to $\rho_o = 0$ in 4(a), black curve, exhibits the behavior that we expect in an homogeneous space, i.e. as expected in the classical formulation of the Vicsek model [28]. This reference curve indicates that in an homogeneous system, the maximum order is reached in the noiseless limit, while as the noise intensity is increased, the order parameter r monotonically decreases until we arrive to the critical noise strength η_{c1} below which the system is fully disorder. Fig. 4(a) shows that the presence of even a small amount of obstacles leads to a qualitatively different picture, with the order parameter r exhibiting a difference behavior with η . All curves with $\rho_o > 0$ reach a maximum at a non-zero value of η , and all decrease as the noiseless limit is approached. This means that for each value of ρ_o , there is an optimal value of η that maximizes collective

³ Since our initial condition is typically a random distribution of particles over space with random moving direction, this average is performed after throwing away a transitory.

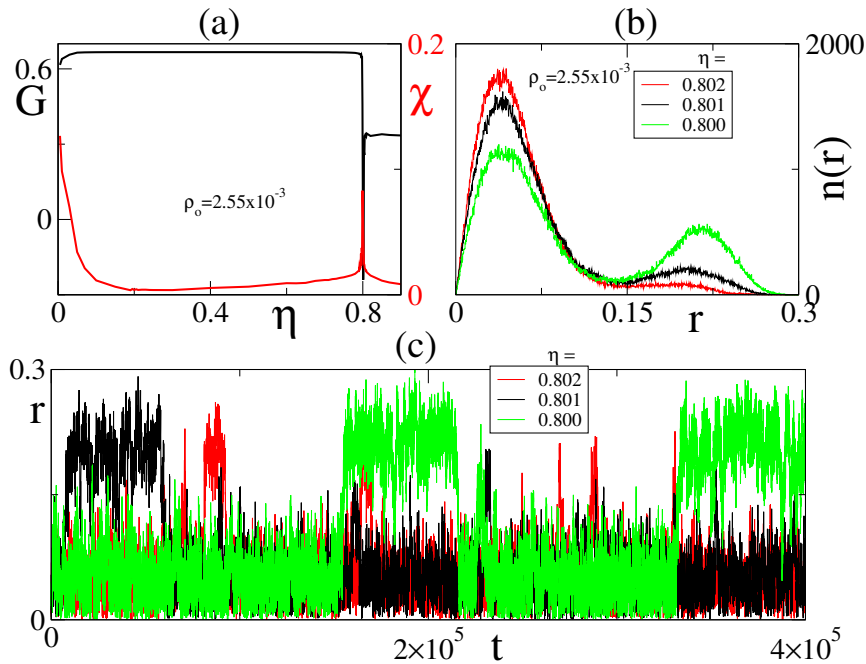


Fig. 5. Evidence of a first-order phase transition at low obstacle densities. (a) Binder cumulant G and susceptibility χ as function of the noise intensity η . Notice that around $\eta \sim 0.8$, G reaches negative values and χ peaks. (b) Histogram $n(r)$ of the order parameter obtained from time series of r . (c) Time series of the order parameter r . Notice the flip-flops in the time series. System size $N_b = 19600$ ($L = 140$).

motion. We referred to this η value as η_M . On the other hand, we observe that if we fix the noise intensity η and vary the obstacle density ρ_o , as display in Fig. 4(b), the order parameter r monotonically decreases as ρ_o is increased. Notice that curves corresponding to different noises exhibit a quite distinct behavior, for instance compare the curve for $\eta = 0.3$, close to the optimal noise η_M for most ρ_o values, with the other curves.

In the following we divide our quantitative analysis into two statical data sets that correspond to low obstacle density and high obstacle density, respectively. We show that at quite small obstacle densities, the numerical data is consistent with a discontinuous (kinetic) phase transition. The numerical data indicates that as the obstacle density increases, the traveling bands become weaker until they disappear. We show that once we reach such obstacle densities, the order is no longer long-range (LRO) in the ordered phase, but rather quasi-long range (QLRO). Our results unambiguously indicate that at such high obstacle densities, as we approach the noiseless limit, i.e. when particles self-organize into densely packed moving clusters as shown in Fig. 2(a), the system is fully disordered, which suggests the existence of a second critical point.

3.1 Low obstacle density

To characterize the phase transition to orientational order at low obstacle density, we introduce two additional quantities, the susceptibility χ and the Binder cumulant [38]

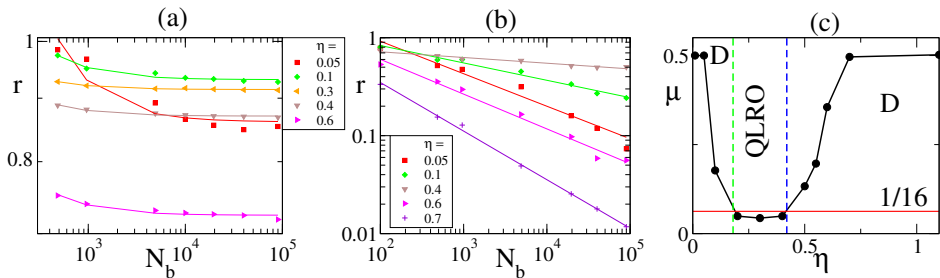


Fig. 6. Finite size analysis at low and high obstacle densities. (a) Scaling of r as function of the system size N_b for low obstacle densities, here $\rho_o = 2.55 \times 10^{-3}$, for various values of η (color coded). The solid lines correspond to exponential fittings: $r(N_b) = r_\infty + C_* \exp(-N_b/N_*)$, with r_∞ , C_* , and N_* fitting constants. Notice that for $N_b \rightarrow \infty$, the order parameter reaches a constant value $r(N_b \rightarrow \infty) \rightarrow r_\infty$, i.e. long-range order (LRO). (b) Scaling of r as function of the system size N_b for high obstacle densities, here $\rho = 0.102$, for various values of η (color coded). The solid curves correspond to power-law fittings: $r(N_b) = A N_b^{-\mu}$, where A and μ are fitting constants. We define, see text, quasi-long-range order (QLRO) when $\mu < 1/16$. On the other hand, $\mu = 1/2$ implies that the system is fully disordered. (c) Exponent μ as function of the noise intensity η for $\rho = 0.102$. The diagram allows us to define two critical points, indicated by the vertical lines: the vertical line to the left corresponds to η_{c2} , while the other one to η_{c1} . In between $\eta_{c2} < \eta < \eta_{c1}$ the order is QLRO. The value $1/16$ is indicated by an horizontal red line.

G , whose definitions are given by:

$$\chi = \langle r^2 \rangle_t - \langle r \rangle_t^2, \quad (5)$$

$$G = 1 - \frac{\langle r^4 \rangle_t}{3 \langle r^2 \rangle_t^2}, \quad (6)$$

We use χ to determine precisely the position of the critical point η_{c1} and G to estimate whether the probability distribution of the order parameter r is unimodal and Gaussian. Notice that the definition of G is directly related to the excess kurtosis. Fig 5(a) shows both quantities as function of the strength η for one of the smallest obstacle densities tested, $\rho_o = 2.54 \times 10^{-3}$. The peak of χ and the sudden change of behavior of G at $\eta = 0.8$ indicates that the critical point is located at $\eta_{c1} = 0.8$. The drop of G to negative values suggests that the probability distribution of r is bimodal [39], as confirmed in Fig. 5(b). This finding is the result of abrupt transitions in the value of r along time, often called “flip-flops”, from low values (disordered gas phase) to high values (ordered phase) and vice versa, Fig. 5(c). In summary, the statical data close to the critical point η_{c1} is consistent with a discontinuous (kinetic) phase transition: negative values of G , a bimodal distribution, and flip-flops as $\eta \rightarrow \eta_{c1}$.

Our next step is to determine whether at low obstacle densities the observed order for $\eta < \eta_{c1}$ remains present in the thermodynamical limit. This involves a finite size scaling. The goal is to obtain the scaling of the order parameter r with the system size. If the system exhibits long-range order (LRO), by increasing the system size, while keeping constant the particle density ρ_b and obstacle density ρ_o , we expect r to saturate to a non-zero value. As measure of the system size we use N_b ⁴. Fig. 6(a) shows that at low obstacles densities, here $\rho_o = 2.55 \times 10^{-3}$, r effectively saturates

⁴ As measure of system size, instead of N_b , we can use either N_o or L . Since ρ_b and ρ_o are constant, knowing either L , N_b , or N_o , we can determine the other two.

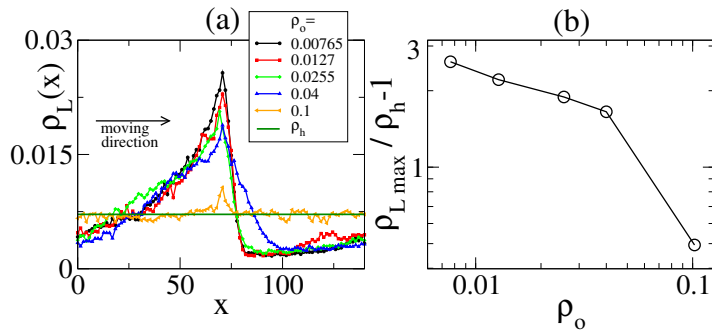


Fig. 7. Bands. (a) The particle density profile $\rho_L(x)$ of the bands along the (band) moving direction. The horizontal line indicates the density profile corresponding to an homogeneous distribution of particles whose value we denote by ρ_h . (b) Maximum $\rho_{L \max}$ of the density profile $\rho(x)_L$ vs. the density of obstacles. The panel shows the quantity $\rho_{L \max} / \rho_h - 1$, which drops to zero for large densities, which indicates the absence of bands in the system.

with N_b to a non-zero value for a large range of $\eta < \eta_{c1}$ values⁵. Thus, the numerical data at very low densities, up to the system size we could reach, is consistent with LRO. This implies that in the thermodynamical limit we expect the system to remain ordered, i.e. as $N_b \rightarrow \infty$, $r \rightarrow r_\infty(\eta) > 0$, where $r_\infty(\eta)$ is the asymptotic value of r in an infinite system, which is a function of η , ρ_b , and ρ_o .

At low obstacle densities, as mentioned above, we observe close to the critical point η_{c1} a behavior consistent with a first-order (discontinuous) phase transition. This seems to be related [31] with the emergence of high-order traveling bands⁶, as shown in Fig. 2(c). Bands are narrow structures that expand through the whole system, elongated in the direction perpendicular to their direction of motion. Several density profiles, corresponding to various ρ_o values, are displayed in Fig. 7(a). To construct these profiles, one needs to project the particle positions onto the moving direction of the band and make a histogram. Bands exhibit a sharp front and a smooth tail. They move across a background gas of disordered (or weakly ordered) particles and accumulate particles in the front as they advance forward, while losing particles in the rear. The presence of obstacles strongly affects bands. As ρ_o is increased, profiles get smoother as illustrated in Fig. 7(a). This can be more quantitatively seen in Fig. 7(b) that shows how the bands vanish for large value of ρ_o . In short, as the number of obstacles is increased, bands become weaker, with a profile that relaxes towards the background gas. At some point, bands and the background gas are undistinguishable and bands vanish. This is evident for $\rho_o > 0.1$, where bands are no longer observed.

3.2 High obstacle density

At high enough obstacle densities, where bands are no longer observed, the system behavior is remarkably different. The finite size study reveals that the system is unable to reach LRO at such high ρ_o values. We find that the order parameter r decays with the system size N_b as a power-law: $r \propto N_b^{-\mu(\eta)}$, where the exponent $\mu(\eta)$ is a function

⁵ Unfortunately, we can not be sure that this behavior remains for $\eta < 0.05$. Smaller noises are hard to explore numerically.

⁶ For instance, when flip-flops are observed, high values of r coincide with the emergence of bands. Along the simulation, bands appear and disappear constantly, as flip-flops do.

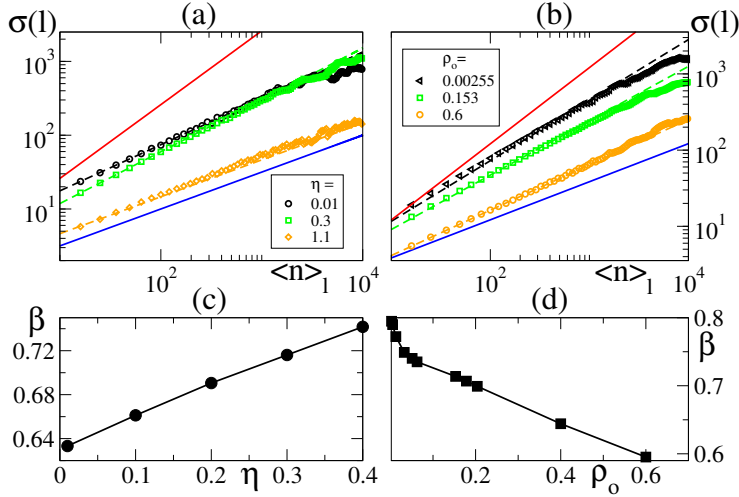


Fig. 8. Number fluctuation statistics. (a) Scaling of the variance of the particle number $\sigma(l)$ vs. the average particle number $\langle n \rangle_l$ for different values of noise strength η for $\rho_o \approx 0.102$. (b) Scaling of $\sigma(l)$ vs $\langle n \rangle_l$ for different values of the obstacle density of obstacles ρ_o and fixed noise strength $\eta = 0.3$. In (a) and (b), the scaling $\sigma(l) \propto \langle n \rangle_l^1$ and $\sigma(l) \propto \langle n \rangle_l^{1/2}$ are indicated by a red and a blue curve, respectively. (c) The dependency of the scaling exponent β (see text for more details) on the noise strength η at fixed $\rho_o \approx 0.102$. (d) The dependency of the scaling exponent β on the density of obstacles at fixed noise strength $\eta = 0.3$. System size $N_b = 40000$ ($L = 200$).

of η , as shown in Fig. 6(b) for $\rho_o = 0.102$. For noises close to the optimal value η_M , we obtain exponent values such that $0 < \mu < 1/16$. Here, by analogy with Kosterlitz-Thouless transition [40] we say that when $0 < \mu < 1/16$ there is quasi-long range order (QLRO), while for $\mu > 1/16$ we assume that the system is disordered. Fig. 6(c) shows that the behavior of $\mu(\eta)$ is such that we can define two disordered phases, one at high noise values and the other one at low noises, and the ordered phase with QLRO at intermediate noises. This implies the existence of two critical points, which obey $\mu(\eta_{ci}) = 1/16$, with $i = 1, 2$ such that $\eta_{c2} < \eta_{c1}$, see Fig. 6(c). The system exhibits QLRO when $\eta_{c2} < \eta < \eta_{c1}$, while being disordered for $\eta < \eta_{c2}$ and $\eta > \eta_{c1}$. Notice that for both disordered phases, μ reaches $1/2$, in particular we observe that $\mu \rightarrow 1/2$ in two limits: $\eta \rightarrow 0$ and $\eta \rightarrow \infty$. A scaling $r \propto N_b^{-1/2}$ corresponds to a fully disordered system with a random distribution of moving directions. Interestingly, the densely packed moving cluster phase at low η values, as the one observed in Fig. 2(a), corresponds, at high obstacle densities, to a fully disordered phase. The presence of only QLRO, or rather the absence of LRO, implies that in the thermodynamical limit we expect $r \rightarrow 0$ for all $\eta > 0$ values, i.e. we expect an infinite system to be disordered. Nevertheless, between $\eta_{c2} < \eta < \eta_{c1}$, we expect the SPPs display large correlations in their moving direction also in the thermodynamical limit.

4 Anomalous density fluctuations and clustering statistics

A way to characterize the distribution of SPPs over the space is through the study of density fluctuations. Particularly useful information is provided by the so-called number fluctuations. The idea is to divide the space over which particles move in cells of linear size l and count the number of particle in each cell. Let us call $n(\mathbf{x}_i, l)$

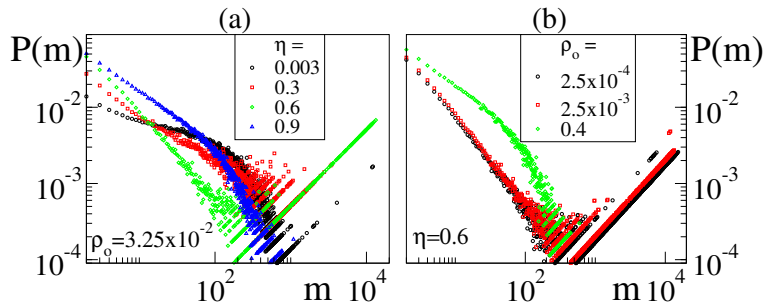


Fig. 9. Clustering statistics. (a) The cluster size distribution $P(m)$ for the fixed density of obstacles $\rho_o = 3.25 \times 10^{-2}$ for different noises η . (b) $P(m)$ for fixed noise value $\eta = 0.6$ and different values of the obstacle density ρ_o . System size $N_b = 19600$ ($L = 140$).

the number of particles in the cell of linear size l whose center is at position \mathbf{x}_i . We are interested in computing the average of this quantity $\langle n(\mathbf{x}_i, l) \rangle_i$ and its standard deviation σ . It is easy to show that $\langle n(\mathbf{x}_i, l) \rangle_i = \rho_b l^2 = \langle n \rangle_l$ and that

$$\sigma(l) = \sqrt{\langle (n(\mathbf{x}_i, l) - \langle n \rangle_l)^2 \rangle_i} = \langle n \rangle_l^\beta, \quad (7)$$

where the average $\langle \dots \rangle_i$ is performed over the cells the space has been divided into. An exponent $\eta = 1/2$ is expected for a random distribution or particles, while $\eta > 1/2$ corresponds to giant number fluctuations (GNF). It has been predicted that in spatially homogenous systems, the SPPs in the ordered phase – far away from the band regime – exhibit GNF [29]. This prediction has been observed in simulations of SPP particles, where a value of $\beta \sim 0.8$ was found [39,41]. Here, we are interested in knowing the impact of an heterogeneous environment on the number fluctuations. Figure 8 shows how number fluctuations are affected by changing the noise intensity η for a fixed density of obstacles $\rho_o \approx 0.102$ (see Fig. 8(a),(c)) and by varying the obstacle density ρ_o while fixing the noise, here $\eta = 0.3$ (see Fig. 8(b),(d)). The top panels of Fig. 8 correspond to the scaling of $\sigma(l)$ with the average number $\langle n \rangle_l$ of particles per cell. In the figure, blue lines correspond to a slope $1/2$, while red line to a slope 1. Undoubtedly, GNF are also present in heterogeneous spaces. Nevertheless, there are important differences with what we know from SPP in homogenous spaces. For instance, for a fixed (high enough) obstacle density ρ_o , GNF are suppressed, or at least decrease, as $\eta \rightarrow \eta_{c2}$, i.e. β adopts smaller values as η approach η_{c2} , Fig. 8(c). We recall that in homogeneous space GNF are expected to be characterized by the same anomalous exponent as $\eta \rightarrow 0$. We also point out that in both homogeneous and heterogeneous spaces, number fluctuations become normal for $\eta > \eta_{c1}$, i.e. in high-noise disordered phase. This means that at high obstacle densities, GNF are stronger at some point in between $\eta_{c2} < \eta_M < \eta_{c1}$, and this seems to occur close to η_M . On the other hand, if we fixed the noise intensity η , we observe that GNF decay as the density of obstacles ρ_o is increased, reflecting the global tendency of the system to go to disorder $\rho_o \rightarrow \infty$. We find that for $\rho_o \rightarrow 0$, $\beta \rightarrow 0.8$ as expected in an homogenous media, while as ρ_o is increased, the exponent β exhibits two regimes with ρ_o , approaching linearly, for high obstacle densities, $1/2$, where fluctuation can be considered normal and the system disordered, see Fig. 8(d).

Another alternative to study how particles are distributed in space is to look at the cluster size distribution. As before, we are interested in understanding how the presence of obstacles affects the non-equilibrium clustering statistics of the SPPs with respect to what we know from homogeneous media [42,43,44]. By “cluster” we understand a group of connected particles, such that the distance between two

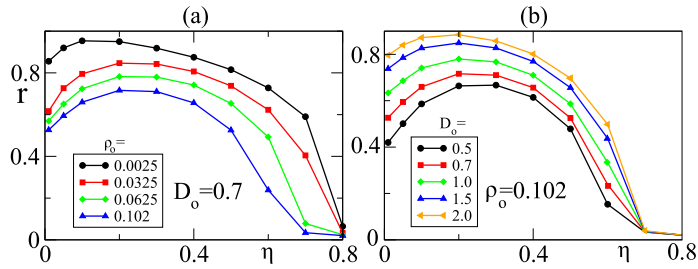


Fig. 10. SPP in a dynamical environment, where obstacles diffuse with a diffusion coefficient D_o . (a) Order parameter r vs. η for various obstacles densities ρ_o and constant diffusion coefficient D_o . (b) r vs. η for constant density of obstacles ρ_o and various diffusion coefficients D_o . Notice that there exist an optimal noise value even in a dynamical environment. System size $N_b = 10000$ ($L = 100$).

connected particles is smaller or equal to the interaction radius. The size or mass of a cluster, which we denote here with the letter “ m ”, is the number of particles the cluster contains. Our quantity of interest is the (weighted) cluster size distribution (CSD) $P(m)$. Its definition is given by:

$$P(m) = \lim_{t \rightarrow \infty} P(m, t) = \lim_{t \rightarrow \infty} \frac{m n_m(t)}{N}, \quad (8)$$

where $n_m(t)$ refers to the number of clusters of mass m that are present in the system at time t . The limit is to indicate that we look at the steady state CSD and neglect transitory behaviors. Fig. 9(a) shows how the CSD is changed by varying the noise η for fixed $\rho_o = 3.25 \times 10^{-2}$. As a reference, the CSD corresponding to a fully disordered phase, i.e. $\eta = 0.9$, is shown. We find that close to η_{c1} the distribution roughly power-law. As we move to lower noise values, $\eta = 0.3$ and $\eta = 0.003$, there is a strong depletion of isolated particles and small clusters and particles tend to form larger clusters, way larger than those observed close to η_{c1} or in the disordered phase (notice the log scale in the figure). There are bigger clusters at $\eta = 0.003$ than at $\eta = 0.3$, despite the fact that the system is more ordered at $\eta = 0.3$ than at $\eta = 0.003$. Fig. 9(b) indicates that by increasing the density of obstacles ρ_o , at fixed noise, here $\eta = 0.6$, the functional form of CSD is dramatically affected. At very large obstacle density, the CSD becomes again similar to the one expected for the disordered phase, which has a well defined average cluster size⁷ and not surprisingly exhibits normal number fluctuations.

5 Discussion: static vs dynamic heterogeneities and the symmetry of the interactions

There is no reason to believe that static and dynamic heterogeneous environments lead to similar large-scale collective effects. In particular, the conclusions drawn from the finite size analysis performed with static obstacles, i.e. with a sort of “quenched” noise, may not apply to dynamical heterogeneities. One may argue that dynamical heterogeneities may be mapped to an effective noise in an SPP system with homogeneous space. In this scenario, the dynamical heterogeneities should not affect qualitatively the large-scale properties of the system but only have an impact on the

⁷ Power-law CSDs may be such that their first moment diverges, while exponential CSDs always have a well defined first moment.

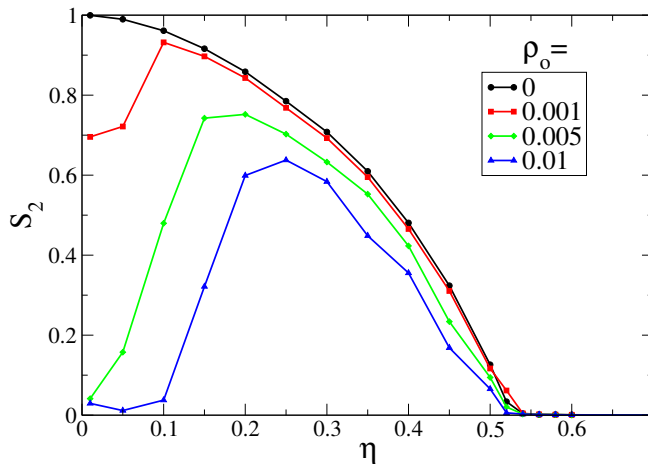


Fig. 11. SPP with nematic alignment in a (static) heterogeneous medium. Nematic order parameter S_2 vs. noise intensity η for different obstacle densities ρ_o . Notice that also SPP with nematic alignment exhibit an optimal noise that maximizes order in the system. System size $N_b = 10000$ ($L = 100$).

critical point. A rigorous analysis would require a finite size study of SPPs in dynamical heterogeneous environments, which is a titanic numerical task out of the scope of the current paper. Less ambitious but not less informative, we can analyze the impact of a dynamical heterogeneous medium on the collective properties of SPPs in a fixed system size. Let us assume that the obstacles now diffuse over the space with a diffusion constant D_o . The position of the k -th obstacle obeys:

$$\dot{\mathbf{y}}_k = \sqrt{2D_o}\xi_k(t) \quad (9)$$

where $\langle \xi_k(t) \rangle = 0$ and $\langle \xi_k(t)\xi_f(t') \rangle = \delta(t-t')\delta_{k,f}$. Fig. 10 shows the order parameter r as function of the (angular) noise η , for various values of ρ_o and fixed obstacle diffusion coefficient $D_o = 0.7$, panel (a), and fixed obstacle density $\rho_o = 0.102$ and various obstacle diffusion coefficient D_o , panel (b). We find that even for a dynamical heterogeneous environment, there is an optimal noise that maximizes collective motion. As the obstacle density is increased, the level of ordering, i.e. r , decreases for all angular noises, Fig. 10(a). On the other hand, we learn that the faster the obstacles diffuse, the weaker the effect of the obstacles, Fig. 10(b). Moreover, the numerical data suggests that in the limit of $D_o \rightarrow \infty$ the system behaves again as an homogeneous system with its critical point shifted to smaller noise values⁸. This suggests that in this limit effectively the problem can be mapped to an homogeneous system with an effective (angular) noise intensity.

Finally, we may wonder whether the observed optimal value is due to the particular symmetry of the velocity alignment between the SPP that has been used, i.e. due to $q = 1$ in Eq. 2. To address this question, we perform simulations with SPP interacting via a nematic velocity alignment, i.e. $q = 2$ in Eq. 2, that move in an heterogeneous medium with static obstacles. Since the alignment is nematic, we replace the order parameter by: $S_2 = \left\langle \left| \frac{1}{N_b} \sum_{i=1}^{N_b} e^{i2\theta_i(t)} \right| \right\rangle_t$, where $\langle \dots \rangle_t$ represents a temporal average after a short transient. For a totally disordered system, $S_2 = 0$, while $S_2 > 0$ implies that the system exhibits, for the tested system size, (global) nematic order. Fig. 11 shows that SPPs interacting via a nematic alignment exhibit, in the presence of an

⁸ Compare Fig. 10(b) and Fig. 4(a), curve for $\rho_o = 0$ to see the shift in the critical point.

heterogeneous environment, an optimal noise η_M as observed above for a ferromagnetic velocity alignment. In this case, the optimal noise η_M maximizes nematic ordering, i.e. it favors the emergence of a preferred direction of motion, where 50% of the SPPs moving roughly parallel to it and the other 50% antiparallel to it. Details about SPPs with nematic velocity alignment in homogeneous media can be found in [36,45,46].

6 Conclusions

We have learned that even small levels of heterogeneity can lead to a qualitative change in the large-scale properties of SPP systems interacting via a velocity alignment mechanism, as first reported in [35]. The presence of obstacles makes more difficult for the SPPs to spread information about their moving direction across the system. Moreover, we observed that by increasing the obstacle density, the level of order always decreases. More importantly, we found that even in weakly heterogeneous systems there is an optimal noise that maximizes collective motion. In addition, we showed that the high-order traveling bands – reported to emerge in the classical, homogeneous, Vicsek model [31,32] – become less pronounced and even disappear as the level of heterogeneities, i.e. obstacles, is increased. At the point where bands are no longer observed, the ordering properties change from long-range to quasi-long range, which suggests that in the limit of an infinite system (keeping constant both, obstacle and particle density), the SPPs cannot coherently cruise the heterogeneous space: i.e. the system is disordered. On the other hand, our finite size analysis revealed that at high obstacle densities, the system exhibits two critical points, one at low and another one at high noise value. Finally, the study of density fluctuations indicated that the giant-number-fluctuation exponent β moves towards $1/2$, which indicates normal density fluctuations, as we approach the noiseless limit, as well as for large enough obstacle densities.

In summary, SPPs moving in static heterogeneous media display new physics unseen in SPP systems in homogeneous spaces. Some of these new features, in particular the existence of an optimal noise that maximizes order, are also present in dynamical heterogeneous media, as well as by changing the symmetry of the velocity alignment mechanism of the SPPs. These findings may prove of great importance for the design and control of artificial and biological active systems.

Finally, it is worth mentioning that few experiments with active particles in heterogeneous media have been already performed, so far with non-aligning active particles: self-propelled Janus particles moving on patterned surfaces [47] and speckle light fields [48,49]. Interestingly, patterned regular environments have been initially used to rectify the motion of active swimmers such as bacteria in diluted suspensions (i.e. in a non-interacting context) [50,51,52]. In these systems, volume exclusion effects and the size of the moving active particles play a central role. Such observations have triggered a good deal of theoretical work. For instance, in simulations with self-propelled disks (SPD) it has been shown that SPDs can get locally jammed by the obstacles [53]⁹, while in simulations with SP rods has been found that V-shaped obstacles can be used to trap particles [54]. On the other hand, it has been shown in simulations with circularly moving active particles that a regular configuration of obstacles can be used to filter the active particles [55,56], while narrow channels can direct particle motion [57]. It remains to be seen how the large-scale collective properties reported here are affected by introducing a velocity alignment mechanism in the above mentioned more realistic models.

⁹ Interestingly, SPD also exhibit an optimal noise that maximizes particle flux [53]. The explanation for this optimal noise seems to be rooted in the local jamming dynamics, being intrinsically different from the one related to the optimal noise value reported here.

References

1. Schaller V, Weber C, Semmrich C, Frey E and Bausch A 2010 *Nature* **467** 73
2. Zhang H, Be'er A, Florin E L and Swinney H 2010 *Proc. Natl. Acad. Sci. USA* **107** 13526
3. Peruani F, Starruss J, Jakovljevic V, Sogaard-Andersen L, Deutsch A and Bär M 2012 *Phys. Rev. Lett.* **108** 098102
4. Buhl J, Sumpter D J T, Couzin I D, Hale J J, Despland E, Miller E R and Simpson S J 2006 *Science* **312** 1402–1406
5. Romanczuk P, Couzin I and Schimansky-Geier L 2009 *Phys. Rev. Lett.* **102** 010602
6. Tunstrøm K, Katz Y, Ioannou C C, Huepe C, Lutz M J and Couzin I D 2013 *PLoS Comput Biol* **9** e1002915
7. Holdo R M, Fryxell J M, Sinclair A R E, Dobson A and Holt R D 2011 *PLoS ONE* **6** e16370
8. Deseigne J, Dauchot O and Chaté H 2010 *Phys. Rev. Lett.* **105** 098001
9. Kudrolli A, Lumay G, Volfson D and Tsimring L 2006 *Phys. Rev. E* **74** 030904(R)
10. Weber C, Thueroff F and Frey E 2013 *arXiv:1301.7701*
11. Jiang H R, Yoshinaga N and Sano M 2010 *Phys. Rev. Lett.* **105** 268302
12. Golestanian R 2012 *Phys. Rev. Lett.* **108** 038303
13. Theurkauff I, Cottin-Bizzone C, Palacci J, Ybert C and Bocquet L 2012 *Phys. Rev. Lett.* **108** 268303
14. Palacci J, Sacanna S, Steinberg A, Pine D and Chaikin P 2013 *Science* **339** 936
15. Golestanian R 2009 *Phys. Rev. Lett.* **102** 188305
16. et al W P 2004 *J. Am. Chem. Soc.* **126** 13424
17. Mano N and Heller A 2005 *J. Am. Chem. Soc.* **127** 11574
18. Rückner G and Kapral R 2007 *Phys. Rev. Lett.* **98** 150603
19. Howse J, Jones R, Ryan A, Gough T, Vafabakhsh R and Golestanian R 2007 *Phys. Rev. Lett.* **99** 048102
20. Golestanian R, Liverpool T B and Ajdari A 2005 *Phys. Rev. Lett.* **94**(22) 220801
21. Bricard A, Caussin J B, Desreumaux N, Dauchot O and Bartolo D 2013 *Nature* **503** 95–98 ISSN 0028-0836
22. Peruani F and Morelli L 2007 *Phys. Rev. Lett.* **99** 010602
23. Romanczuk P, Bär M M, Ebeling W, Lindner B and Schimansky-Geier L 2012 *Eur. Phys. J. Special Topics* **202** 1
24. Alberts B, Bray D, Lewis J, Raff M, Roberts K and Watson J 1994 *Molecular biology of the cell* (Garland publishing)
25. Dworkin M 1993 *Myxobacteria II* (Amer Society for Microbiology)
26. Marchetti M C, Joanny J F, Ramaswamy S, Liverpool T B, Prost J, Rao M and Simha R A 2013 *Rev. Mod. Phys.* **85** 1143–1189
27. Ramaswamy S 2010 *Annual Review of Condensed Matter Physics* **1** 323–345
28. Vicsek T and Zafeiris A 2012 *Physics Reports* **517** 71–140
29. S Ramaswamy R A S and Toner J 2003 *Europhys. Lett.* **62** 196–202
30. Vicsek T, A Czirok E, Jacob E B, Cohen I and Shochet O 1995 *Phys. Rev. Lett.* **75** 1226
31. Grégoire G and Chaté H 2004 *Phys. Rev. Lett.* **92** 025702
32. Caussin J B, Solon A, Peshkov A, Chaté H, Dauxois T, Tailleur J, Vitelli V and Bartolo D 2014 *Phys. Rev. Lett.* **112** 148102
33. Toner J and Tu Y 1995 *Physical Review Letters* **75** 4326–4329
34. Toner J and Tu Y 1998 *Phys. Rev. E* **58** 4828
35. Chepizhko O, Altmann E G and Peruani F 2013 *Phys. Rev. Lett.* **110**(23) 238101
36. Peruani F, Deutsch A and Bär M 2008 *Eur. Phys. J. Special Topics* **157** 111
37. Chepizhko O and Peruani F 2013 *Phys. Rev. Lett.* **111**(16) 160604
38. Binder K 1997 *Reports on Progress in Physics* **60** 487
39. Chaté H, Ginelli F, Grégoire G and Raynaud F 2008 *Phys. Rev. E* **77** 046113
40. Kosterlitz J M and Thouless D J 1973 *Journal of Physics C: Solid State Physics* **6** 1181
41. Dey S, Das D and Rajesh R 2012 *Phys. Rev. Lett.* **108**(23) 238001
42. Peruani F, Deutsch A and Bär M 2006 *Phys. Rev. E* **74** 030904(R)

43. Peruani F, Schimansky-Geier L and Bär M 2010 *Eur. Phys. J. Special Topics* **191** 173–185
44. Peruani F and Bär M 2013 *New J. Phys.* **15** 065009
45. Ginelli F, Peruani F, Bär M and Chaté H 2010 *Phys. Rev. Lett.* **104** 184502
46. Peshkov A, Aranson I, Bertin E, Chate H and Ginelli F 2012 *Phys. Rev. Lett.* **109** 268701
47. Volpe G, Buttinoni I, Vogt D, Kummerer H J and Bechinger C 2011 *Soft Matter* **7** 8810–8815
48. Paoluzzi M, Leonardo R D and Angelani L 2014 *Journal of Physics: Condensed Matter* **26** 375101
49. Volpe G, Volpe G and Gigan S 2014 *Scientific Reports* **4** 3936
50. Galajda P, Keymer J, Chaikin P and Austin R 2007 *J. Bacterial.* **189** 8704
51. Wan M, Reichhardt C O, Nussinov Z and Reichhardt C 2008 *Phys. Rev. Lett.* **101** 018102
52. Tailleur J and Cates M 2009 *Europhys. Lett.* **86** 60002
53. Reichhardt C and Olson Reichhardt C J 2014 *Phys. Rev. E* **90**(1) 012701
54. Kaiser A, Wensink H and Löwen H 2012 *Phys. Rev. Lett.* **108** 268307
55. Mijalkov M and Volpe G 2013 *Soft Matter* **9** 6376–6381
56. Reichhardt C and Reichhardt C J O 2013 *Phys. Rev. E* **88**(4) 042306
57. Radtke P and Schimansky-Geier L 2012 *Phys. Rev. E* **85** 051110